Avalanches in the 3D-GRFIM with metastable dynamics: Finite-size Effects on critical exponents

Jordi Baró i Urbea
tutor: Eduard Vives Santa-Eulalia

Abstract

The Sorted-List algorithm for the simulation of a 3D-GRFIM has been implemented in C++ and executed in DIRAC Iberian grid in order to obtain distributions of size and duration of magnetization avalanches. We have performed maximum-likelihood estimations of the power-law exponents. We have obtained 2D-exponent maps by scanning the upper and lower bounds of the distribution. We have used the maps to compare the behaviour of two different methods for classifying percolating avalanches and evaluate the dependence of the exponent with the disorder parameter R and the size of the lattice L.

KeyWords: 3D-Gaussian Random Field Ising Model, Sorted-List, Avalanche Dynamics, Max. Likelihood, Criticality

I. Introduction

First order phase transition in many condensed matter experimental systems like ferromagnets[1] or ferroelastics[2] need to be described under the paradigm of athermal systems with quenched disorder. We can identify them by the presence of an intermittent response in the order parameter when the system is driven by a smoothly varying external force. This phenomenon is called avalanche dynamics.

When a first order phase transition is induced at low temperature the system is trapped in a metastable state while the potential barriers are much higher than the thermal fluctuations. In the athermal limit only when the barriers disappear the system is able to jump suddenly in an avalanche process from a metastable minimum to a more stable one. This leads to the splitting of the equilibrium transition discontinuity line into a rate-independent hysteresis loop. Furthermore the presence of quenched disorder distorts the energy landscape. Instead of two metastable states the free energy of the system exhibits a series of local metastable states through which the system will jump. The hysteresis loop is then tilted and smoothed to a nearly continuous but still rate independent loop.

In this work we will focus in the study of a disordered ferromagnet within this athermal paradigm. We are going to describe it by the zero-temperature Random Field Ising Model (RFIM) with metastable dynamics, introduced by H. Ji and Mark Robbins[3]

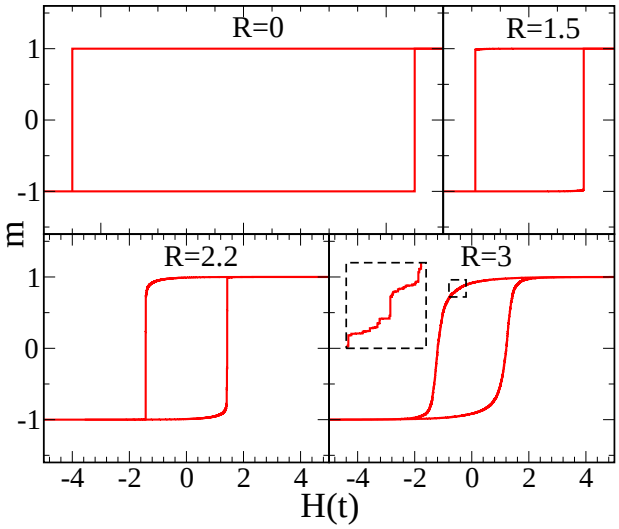

Figure 1: *Hysteresis loops for different amounts of disorder R. Even a small disorder generates a non trivial avalanche process. Infinite avalanches occur for low disorder until the critical value R_c is overtaken. The inset shows a detail of the loop where sudden Barkhausen jumps are revealed.*

to study fluid invasion in porous media and front propagation in disordered systems and later used by Sethna et al. [1] as a prototype model for the study of avalanche dynamics. This model is able to reproduce the following characteristics in a ferromagnetic first order transition that thermal models cannot explain: Rate independent hysteresis, the Return-Point Memory effect[4] and the Barkhausen noise[6][7].

Fig.1 shows different examples of hysteresis loops obtained by the simulation of non-equilibrium metastable dynamics in the 3D version of RFIM with Gaussian distributed disorder (3D-GRFIM). Details of the model are given in the next section.

Tuning the amount of disorder R (standard deviation of the Gaussian) we find a transition between two regimes (see fig.1):
(a) For low disorder ($R = 1.5$) most of the magnetization change is associated to a giant percolative avalanche that propagates through the whole system. In the $R = 0$ limit the model reproduces a square Preisach-like loop [8].
(b) For large disorder ($R = 3$) the hysteresis loop seems smoothed and tilted although it is still formed by a sequence of small avalanches as shown in the inset of fig.1.
When the disorder is close to a critical value $R_c \sim 2.2$ the avalanches exhibit a size distribution which is scale-free.

II. The Random Field Ising Model: details

The 3D-GRFIM is based on the original Ising model with the addition of a random internal field h_i acting on each spin s_i. The values h_i are quenched and distributed according to a gaussian density $\rho(h)dh = \frac{1}{\sqrt{2\pi}R} e^{\frac{-h^2}{2R^2}} dh$ with zero mean and variance R^2. The hamiltonian of the system (considering first neighbours interaction) reads:

$$\mathcal{H} = -J \sum_{\langle i,j \rangle} s_i s_j - \sum_{i}^{N} (H(t) + h_i) s_i \qquad (1)$$

where $s_i = \pm 1$ are spin variables defined on a regular lattice.

Several works have studied this model using the standard thermal equilibrium dynamics[9]. In our case we use the metastable dynamics. It can be seen as a limiting version of the Glauber spin-flip dynamics at zero-Temperature. The local Hamiltonian of each spin reads:

$$\mathcal{H}_i = s_i \left(-J \sum_{\langle j \rangle} s_j - H(t) + h_i \right) \qquad (2)$$

Each individual spin flips minimizing this local Hamiltonian. This leads to the following rule:

$$s_i = sign\{ J \sum_{\langle i,j \rangle} s_j + H(t) + h_i \} \qquad (3)$$

Each flip may occur in two ways: by changing the state of it's neighbours $\{s_j\}$ within the propagation of an avalanche; or by seeding a new one due to a change in the external field $H(t)$.

III. Simulation Details

All simulations have been done using a C++ code developed specifically for this work and later executed in DIRAC iberGrid. The regular lattice is stored as a 3D array (sized $L \times L \times L$) of C++ Objects containing it's direction s_i and internal field h_i and a method returning the total force exerted by their neighbours according to periodic boundary conditions.

The internal fields h_i are obtained from a Box-Muller[11] algorithm for gaussian numbers generated over a set of uniform random numbers generated by RANECU[10]. In order to check their correct distribution we performed a Kolmogorov–Smirnov test on the 95% confidence interval. An example of the results is shown in fig.2.

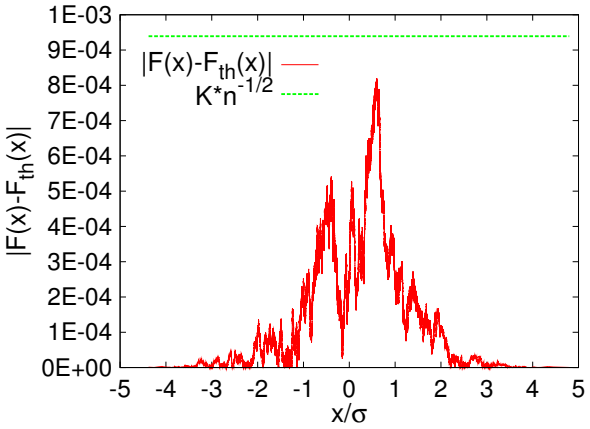

Figure 2: *Kolmogorov-Smirnov test over the gaussian numbers. Red line shows the difference between the theoretical and the experimental cumulative distribution function. Green line shows the threshold for 95% confidence*

In order to implement the metastable dynamics we take advantage of the adiabaticity of the model; Instead of smoothly increasing the external field, the code does the following:
1. Finds which one among the unflipped spins will start the first avalanche according to eq(3).
2. Sets the next external field to the triggering value.
3. Propagates this avalanche.

4. Find the next triggering spin and iterates the process.
In this way the magnetization process is obtained as the trajectory from the configuration corresponding to magnetization $M = -N$ to the one corresponding to $M = N$ forming the loops shown in fig.1.

The propagation of a single avalanche is organized in shells. The triggering spin (Shell-0) will change the force acting over it's neighbours. Some of them may flip constituting Shell-I; again this shell changes the force acting on its neighbours. The spins that flip by the influence of shell-N will constitute the Shell-N+1. The number of spins in each shell represents the profile of the avalanche in time $V(t)$ characterizing the Barkhausen noise. Fig.3 shows a typical avalanche profile. Assuming that these profiles obey a scaling rule[13] according to it's duration: $\langle V(t,T)\rangle = T^b\langle V(t/T)\rangle$. One can find a universal relation between the typical size of an avalanche and it's duration: $\langle S(T)\rangle = \int_0^T \langle V(t,T)\rangle dt = S_0 T^{b+1}$.

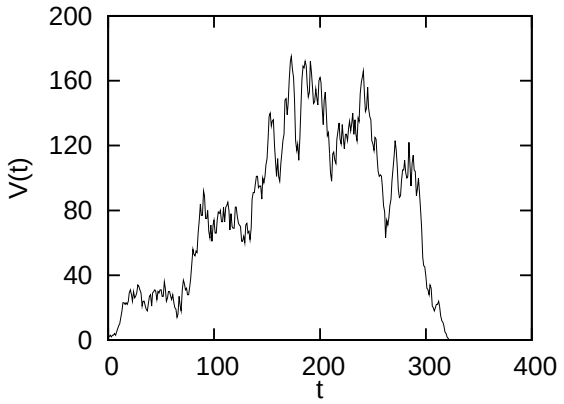

Figure 3: *Typical profile V(t) of a critical avalanche in an L=32 lattice and R=2.19*

The hot spot of the simulation is the search of the next triggering spin. It will correspond to the unflipped spin with the smallest internal field. The brute-force method consist in scanning over the whole lattice for each avalanche. This method is slow to run but has also been implemented to use it as a reference for the next more sophisticated algorithm.

IV. The Sorted-List algorithm

An important speed improvement can be obtained with the implementation of the sorted-list algorithm[12].This method work as follows:
1. List all the spins of the lattice sorted by it's internal field from lowest to highest values.
2. Build an array of seven pointers $nPos[k]$ to the first element in the list that needs $k = \{0, 1, .., 6\}$ neighbours up to flip according to its internal field. The next triggering spin will be pointed by one member of $nPos$.
3. Among $nPos[k]$ we check which one would need the smaller external field to flip if it have k neighbours flipped.
4. We check if it actually have exactly k neighbours flipped. If not: either it has more neighbours flipped and have already been flipped; or else k isn't reached and as the needed external field will be exceeded in the next avalanche it will flip inside another avalanche or will eventually be reached by the pointer $nPos[k-1]$. We can then advance the pointer one site in the sorted-list, and iterate step 3
5. One of the pointers will finally find k neighbours flipped. This spin will trigger the new avalanche. The code set the new external field to the one needed to flip this triggering spin and advance the pointer $nPos[k]$.

The improvement in execution time obtained with this method is shown in Fig.4.

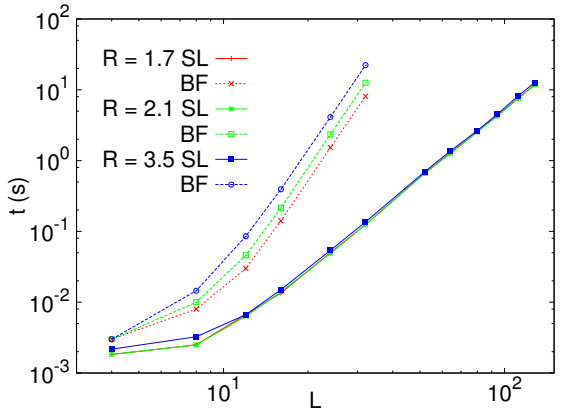

Figure 4: *Comparison between the execution time of the two simulation methods (Sorted-List and Brute-Force) for one magnetization process in lattices of different size*

This code can be used to evaluate many aspects of the RFIM. We have focused on the analysis of size and duration distribution of the avalanches considering different classifications of the percolating ones (avalanches discussed in section VIII that span the whole lattice at least in one axis: x, y, z). We have simulated 2000 magnetization processes for values of R ranging from $R = 1.85$ to $R = 2.56$ and lattice sizes ranging from $L = 32$ to $L = 256$.

V. Criticality

The distribution of sizes of the finite avalanches was proposed[1] to have a universal behaviour near the critical disorder R_c as a function of the reduced external field $h \equiv \frac{H-H_c}{H_c}$ and reduced disorder $r \equiv \frac{R-R_c}{R_c}$:

$$D(S,r,h) = S^{-\tau}\mathcal{D}_{\pm}(S/|r|^{-1/\sigma}, h/|r|^{\beta\delta}) \qquad (4)$$

Where $\mathcal{D}_{\pm}(x,y)$ is a universal scaling function considering the cut-off $|r|^{-1/\sigma}$ and exponents $\beta\delta$ that define the scaling over magnetization $M(h,r) = |r|^{\beta}\mathcal{M}_{\pm}(h/|r|^{\beta\delta})$. Th density $D(S,r,h)$ will converge to the power law $S^{-\tau}$ in the critical limit $r \to 0$, $h \to 0$.

We can find the expected distribution along the full hysteresis cycle by integrating this expression over all values of h:

$$\overline{D}(S,r) = \int_{-\infty}^{\infty} D(S,r,h)dh =$$

$$= S^{-\tau}r^{\beta\delta}\int \mathcal{D}_{\pm}(S/|r|^{-1/\sigma}, z)dz =$$

$$= S^{-\tau-\beta\delta\sigma}\left(S/|r|^{-1/\sigma}\right)^{\beta\delta\sigma}\overline{\mathcal{D}}_{\pm}(S/|r|^{-1/\sigma})$$

$$\overline{D}(S,r) = S^{-\tilde{\tau}}\tilde{\mathcal{D}}_{\pm}(S/|r|^{-1/\sigma}) \qquad (5)$$

Where $\tilde{\tau} = \tau + \sigma\beta\delta$ will then be the critical exponent for the distribution of sizes integrated over a whole magnetization process.

As stated in section III we expect also a scale-free relation between T and S. The avalanche duration T behave as $T \propto L^z$. The fractal dimension of the critical avalanches is $\sigma\nu$ ($S \propto L^{\sigma\nu}$)It can be found[13] that $\langle S(T)\rangle = S_0 T^{\frac{1}{\sigma\nu z}}$ and then the scaling of the universal relation in avalanche profiles has the exponent $b = \frac{1}{\sigma\nu z} - 1$. The distribution of durations can be obtained from the relation $S(T) \sim S_0 T^{\frac{1}{\sigma\nu z}}$. Performing a change of variable:

$$D(T,r) = D(S,r)|\frac{dS}{dT}| \sim S^{-\tau}\mathcal{D}_{\pm}(S/|r|^{-1/\sigma})T^{\frac{1}{\sigma\nu z}-1}$$

$$D(T,r) =\sim T^{-\frac{\tau-1}{\sigma\nu z}-1}\mathcal{D}_{\pm}(T^{\frac{1}{\sigma\nu z}}/|r|^{-1/\sigma})$$

$$D(T,r,h) = T^{-\alpha}\mathcal{D}_{\pm}(T/|r|^{-\sigma\nu z/\sigma}, h/|r|^{\beta\delta}) \qquad (6)$$

Where $\alpha = (\tau-1)/\sigma\nu z + 1$. Again, we can obtain the behaviour over the whole magnetization process:

$$\overline{D}(T,r) = T^{-\tilde{\alpha}}\tilde{\mathcal{D}}_{\pm}(T/|r|^{-\nu z}) \qquad (7)$$

where $\tilde{\alpha} = \alpha + \beta\delta/\nu z = \frac{\tau+\sigma\beta\delta-1}{\sigma\nu z} + 1$

Exponents have been already estimated in previous works[14] with different methods and are still controversial:

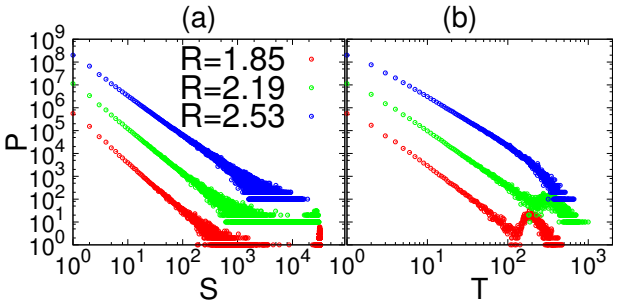

Figure 5: *Distribution of avalanche sizes (upper) and durations (lower) for different values of R in a L=32 lattice*

exponent	simulation 3D
τ	1.60 ± 0.06
$\tilde{\tau}$	2.03 ± 0.03
α	2.05 ± 0.12
$\tilde{\alpha}$	2.81 ± 0.11

VI. Estimation procedure for the critical exponents

An statistical estimator is needed in order to determine the best fit for the exponents $\tilde{\tau}$ and $\tilde{\alpha}$. Graphical methods like linear least square fail to estimate the exponent of a power-law distribution. A maximum likelihood (ML) method will provide more much accurate results[16]. The power law distribution we want to fit is:

$$p(k) = \frac{k^{-\gamma}}{\sum_k k^{-\gamma}} \qquad k = 1, ..., L^3 \qquad (8)$$

In this work we want to evaluate the effects of the finite size of the lattice by cutting the distribution from k_{min} to k_{Max}. Then $p(k) = \frac{k^{-\gamma'}}{\sum_k k^{-\gamma'}}$ where $k = \{k_{min}, ..., k_{Max}\}$. The likelihood function reads:

$$\ln \mathcal{L}(\gamma'; k_m, k_M) = -\gamma' \sum_{\mathrm{k}=k_m}^{k_M} f(\mathrm{k})\ln(\mathrm{k}) - N\ln\left(\Sigma\, \mathrm{k}^{\gamma'}\right)$$

where $f(k)$ is the frequency of occurrence of k obtained in the simulation. As we are interested in the numerical maximization of that function the best value of γ' can be found from its derivative:

$$\frac{\partial\mathcal{L}}{\partial\gamma'} = -\sum_{\mathrm{k}=k_m}^{k_M} f(\mathrm{k})\ln(\mathrm{k}) + N\frac{\sum_{k_m}^{k_M}\mathrm{k}^{\gamma'}\ln(\mathrm{k})}{\sum_{k_m}^{k_M}\mathrm{k}^{\gamma'}} \qquad (9)$$

We solve $\frac{\partial\mathcal{L}}{\partial\gamma'} = 0$ by the false position method.

The effect of the anomalies in the upper and lower values can be managed by tuning the minimum and

maximum range, k_{min} and k_{Max}. Previous numerical works consider the upper bound anomalies as a consequence of the lack of statistics and study the effect of the small avalanches by varying k_{min}. In this work we will consider the changing of the upper bound as well and construct the 2D-exponent maps.

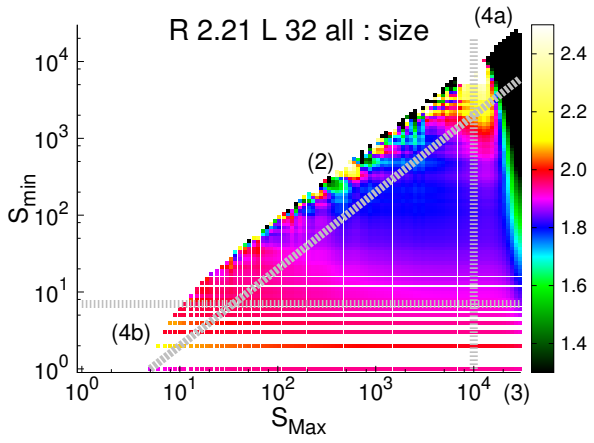

Figure 6: *Sample 2D-exponent map where the different exclusion regions have been identified: (2) low statistics; (3) estimation with the full distribution(4a); effect of percolating avalanches; (4b) effect of small avalanches*

VII 2D-Exponent Map

The 2D-exponent maps shown in this work correspond to the exponents $\tilde{\tau}$ and $\tilde{\alpha}$ estimated by maximum likelihood, restricting the data to the interval between a minimum and maximum avalanche size (S_{min}, S_{Max}) or a minimum and maximum duration (T_{min},T_{Max}).

This method tries to provide a visual representation of these distributions. The main goal is to evaluate simultaneously the upper and lower anomalies and identify the flat region (constant exponent) that obeys the expected scale-free distribution. In addition it also provides an alternative representation of the distribution without loosing major local information.

Fig.6 shows an illustrative example where some properties of the map can be identified:
(1) The axis of the map correspond to the upper and lower cut-off's. Thus, each point in the diagram correspond to a (S_{Max}, S_{min}) pair. The color indicate the value of the exponent obtained by Maximum Likelihood from the data within this interval. We

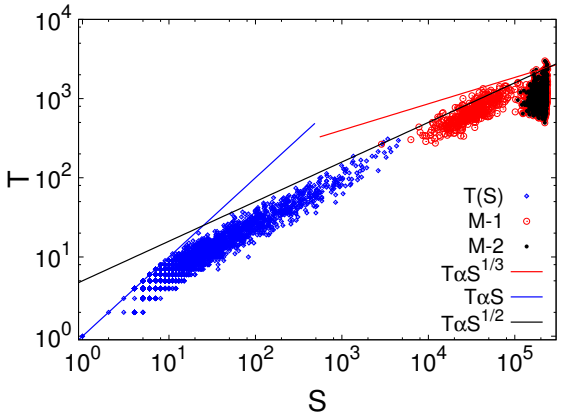

Figure 7: *Diagram showing the relation between avalanche durations T and sizes S. Blue dots correspond to all the avalanches obtained from the simulation of one realization of disorder with size $L = 64$ and $R = 2.56$. The blue line indicates the minimum propagation speed ($T < S$) and the black line correspond to the expected law $\langle S(T)\rangle \propto T^{\frac{1}{\sigma\nu z}}$. Red points show all the spanning avalanches obtained from the simulation of 2000 realizations of disorder with $R = 1.15$ and $L = 64$. Black points are the infinite avalanches classified by method-2.*

choose a geometrical discrete growing separation between the evaluated points $S^{i+1}_{min} = a\, S^{i}_{min}$. So that the points are uniformly distributed in the logarithmic scale.
(2) Diagonal lines $\Gamma(\Delta)$ represented in fig.6 correspond to the points such that $S_{min} = S_{max}/\Delta$. This means a fixed interval $ln\Delta$ in logarithmic scale. Lower values of Δ will be affected by the lack of statistics and present a rough profile (region (2)) while higher values close to point (3) contain less local information but correspond to higher statistics.
(3) The bottom-right corner corresponds to the value of the exponent obtained by considering all the data set: S_{min}=1 and $S_{Max} = max\{S\}$. This estimation will be affected by upper and lower anomalies and thus will return a wrong value.
(4) The upper-right (4a) and lower-left(4b) corners are highly affected for the populations that drive the distribution away from the power law. These anomalies delimit a threshold for S_{min} and S_{max} indicated by the vertical and horizontal dashed lines beyond which all data is affected in some degree by the anomaly.
(5) A flat region is expected to appear between the anomalous thresholds, excluding both upper and lower anomalies (4a,4b) and the noisy region (2). We

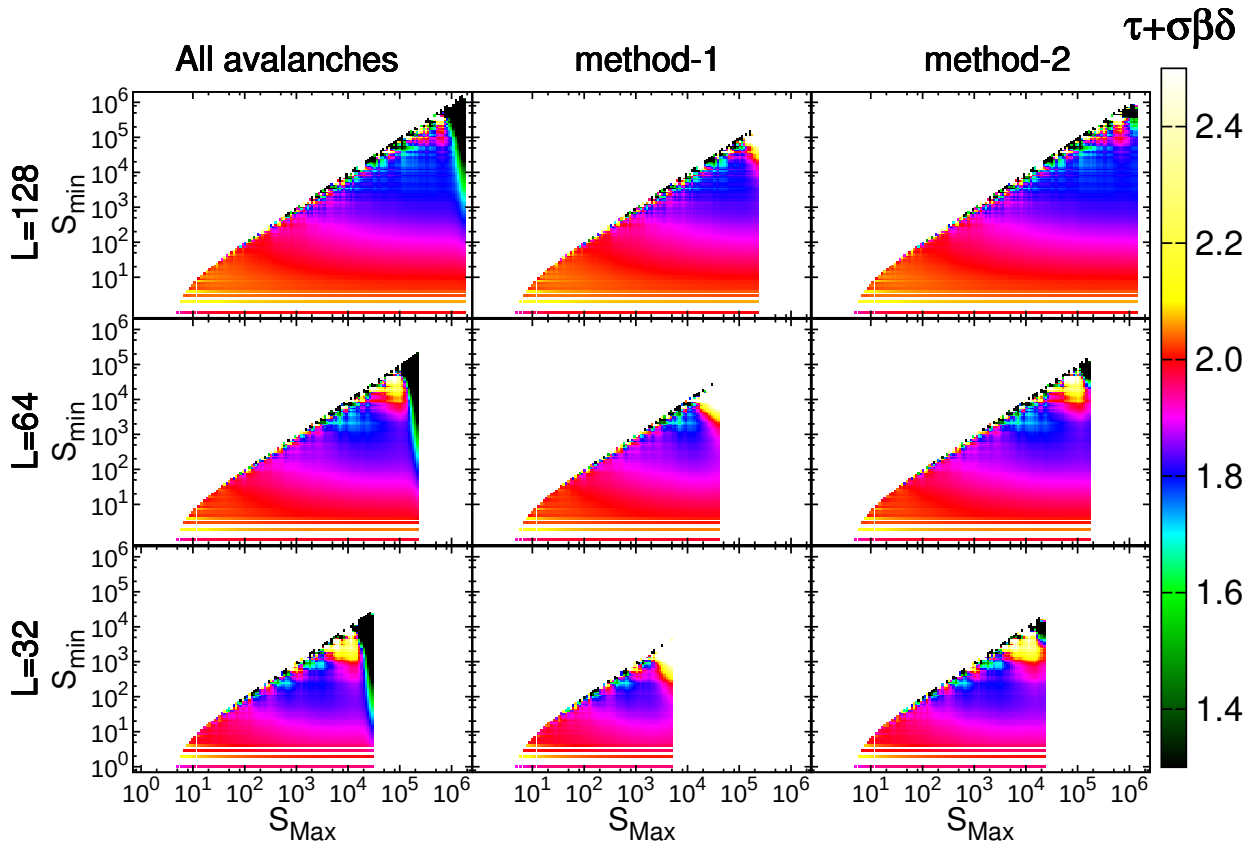

Figure 8: *These 2D-exponent maps obtained for a fixed $R = 2.19$ illustrate the decision of taking method-2. If no classification is done, infinite avalanches distorts the estimation for all values of S_{Max} above the size where they collapse. Method-1 cuts too soon the distribution, leave too poor statistics and still distorts the exponent for high S_{Max}. Method-2 instead allows a long ranged estimation that can be corroborated in comparison with larger lattices*

consider the crossing of the thresholds as the best value for the exponent because is the one with higher statistics.

The origin of the anomalies is identified in fig.7. Scale-free avalanches are distributed according to the statistical relation: $T \propto S^{\sigma\nu z} \sim S^{0.5}$. The small avalanches affected by the discrete nature of the lattice are unable to spread slower than $T = S$. Finally percolating avalanches discussed in the next section show a size S that saturates below the size of the mesh L^3.

VIII. Classification of the Spanning Avalanches

In the theoretical framework (for $L \to \infty$) we should be able to distinguish three different kinds of avalanches[17]:
Infinite massive avalanches: Only occur below the critical point R_c. These avalanches are expected to scale with the size like $S \propto L^d$.
Critical massless avalanches: Occur in the critical point R_c. Scale by a fractal dimension $S \propto L^{1/\sigma\nu}$[13]
Finite avalanches: corresponding to the vast majority in any magnetization process both above and below R_c. These avalanches are distributed according to eq(5) and eq(7).

When we consider finite size systems this classification is not possible and the avalanches can be only separated between two groups: percolating and non-percolating. In order to evaluate the behaviour of finite avalanches we need a way to identify which among the percolating avalanches would correspond to the infinite massive ones in the thermodynamic limit and discard them. In this work we will consider two different criteria:
Method-1: We discard all spanning avalanches: those covering the whole length of the system in at least one dimension of the space.
Method-2:[17] We discard only those avalanches spanning over the three dimensions if they are unique in the magnetization process. If more than one 3D-spanning avalanche are found in a magnetization process we consider that they're both finite ones

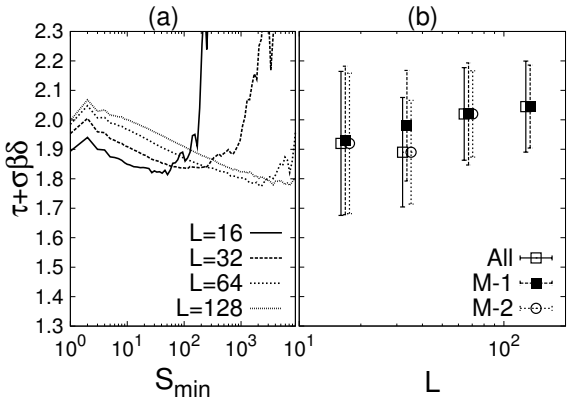

Figure 9: *(a) $\tilde{\tau}(k_{min})$ cuts for different sizes according to classification method-2 for $R = 2.19 \sim R_c$. (b) Position of the pick of the histogram of frequencies obtained for all three methods and for different sizes. The resulting exponent seems to converge towards $\tilde{\tau} \sim 2.05$*

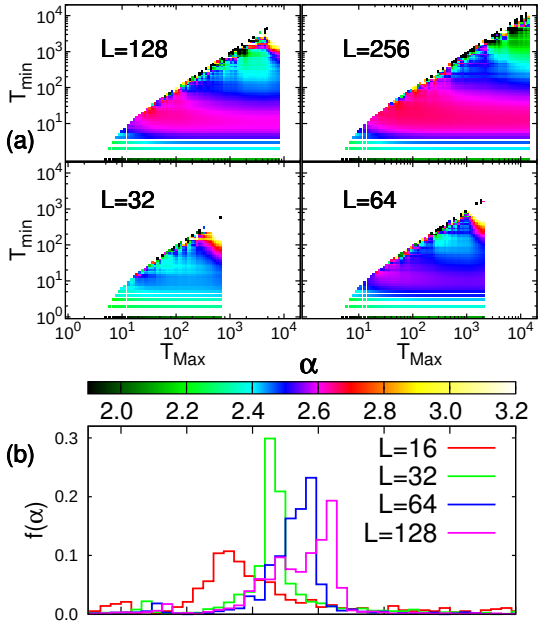

Figure 10: *(a) 2D-exponent maps of distribution of durations. Upper and lower bound anomalies are stronger here even for M-2 classification. (b) Frequencies of exponents $\tilde{\alpha}$ found in each size. As discussed, the peak of maximum frequency gets closer to the expected 2.8 as the lattice grows.*

and none of them is discarded. This is based on the underlying idea that it is impossible to have two infinite avalanches in the same process.

Fig.7 compares the avalanches discarded by method-1 (red) and method-2 (black). Most of the avalanches classified as percolating by method-1 still follow the behaviour expected for the scale-free ones. Method-2 seems to accept some percolating avalanches as good ones.

In fig.8 we compare the goodness of both classification methods by using 2D-exponent maps. We have found that method-2 increases the area that converges to a power-law distribution. For lattices of the same size we retrieve more useful data than using method-1 or no classification. In fig.8 one also can observe the effect of increasing L.

IX. Discussion about the value $\tilde{\tau}$

We use the results shown in fig.8 to evaluate $\tilde{\tau}$ using the (S_{min},S_{Max}) scanning. Now that we have confirmed the goodness of method-2 classification we will check the classical $\tilde{\tau}(S_{min})$ cuts for a better visualization (fig.9). Instead of the expected power-law we find an slightly decreasing exponent. Also these k_{min} cuts show that the obtained exponent depends on the size of the mesh. All this points to the existence of a small dependence on the size of the mesh as previous studies[17] have already pointed out.

We also observe that for small avalanches the results seem to present a broad oscillation, enlarging the distribution of even avalanche sizes. This effect can be caused by the discrete nature of the lattice that still remain unstudied.

In order to obtain an estimation of the exponent according to these results we have chosen the following criteria: We have built an histogram of the obtained exponents in the 2D-exponent map for the logarithmic binning and select the most frequent (median) of them. We have selected the variance of the obtained histogram as the error of the estimation.

X. Scaling of the distribution of durations

For the evaluation of the distribution of durations we extend the size range up to $L = 256$. We find that the anomalies are much more relevant both for small and percolating avalanches as shown in fig.10. As percolating avalanches are quicker than the scale-free, their distortion begin at short times. Also short avalanches have a exponent lower than expected. Even though we can use the frequencies (insets of figure 10) to find an approximate estimation for the best value for each L. We see a broadening of the peak that may be caused

by a finite size scaling rule.

XI. Conclusions

In this work we have studied the distributions of time and duration of the avalanches occurring in a lattice of spins with quenched disorder. We have simulated the non-equilibrium athermal dynamics of the 3D-GRFIM for different lattice size L and disorder parameter R.

The sorted-list algorithm used in the simulation improved the execution time, allowing us to obtain statistically relevant data for lattices up to L=256 (16,777,216 spins).

The resulting avalanche distributions have been compared to a power-law distribution function using a maximum likelihood method. We have developed the 2D-exponent map as a visualization technique for evaluating the local anomalies on the exponent caused by the finite size of the mesh as well as the discrete nature of the simulation. The method may also be useful for the evaluation of other parameters estimated from a given numerical distribution. Once the anomalous region has been identified we can subtract it in order to obtain a result in the well behaved region.

For the case of the 3D-GRFIM removal of infinite massive avalanches helps to improve the fit to the power-law. We have compared two methods for classifying the infinite avalanches. Method-2 (selecting only the unique avalanche spanning through 3 dimensions) has proven to give a larger range of valid data than method-1 (selecting all avalanches spanning in at least 1 dimension) or no classification.

The obtained value of the exponent have not fully agreed with the expected ones from the literature. For lattices of finite size we have found that probability densities show a small drift to the expected power-law, at least for the sizes evaluated in this work. However the convergence to $\tilde{\tau} \sim 2.02$ and $\tilde{\alpha} \sim 2.81$ for $L \to \infty$ seems plausible with the data obtained.

Finally, more detailed results and discussion with statistically richer data and larger lattices are expected to be obtained in future studies.

References

[1] James P. Sethna, Karin Dahmen, Sivan Kartha, James A. Krumhansl, Bruce W. Roberts, and Joel D. Shore, *Phys. Rev. Lett.* ***70***, 3347–3350 (1993)

[2] Francisco J. Pérez-Reche, Eduard Vives, Lluís Mañosa, and Antoni Planes *Phys. Rev. Lett. 87*, 195701 (2001)

[3] M. O. Robbins and H. Ji, *Phys. Rev. B* ***46*** 14519 (1992)

[4] D. C. Jiles and D. L. Atherton, *J. Appl. Phys.* ***55***, 2115 (1984)

[5] Yang Liu and Karin A. Dahmen *Phys. Rev. E* ***76***, 031106 (2007)

[6] H. Barkhausen, *Phys. Z.* ***20***, 401 (1919)

[7] Spasojević, Djordje and Bukvić, Srdjan and Milošević, Sava and Stanley, H. Eugene, *Phys. Rev. E* ***54***, 3 2531–2546 (1996)

[8] F Preisach *Z. fur Phys.* ***94***, 277 (1935)

[9] Francesc Salvat-Pujol and Eduard Vives *Phys. Rev. E* ***79***, 061116 (2009)

[10] F. James, *Comp. Phys. Comm.* ***60***, p 329-344 (1990)

[11] Box, G. E. P. and Muller, M. E. *"A Note on the Generation of Random Normal Deviates." Ann. Math. Stat.* ***29***, 610-611 (1958)

[12] Matthew C. Kuntz, Olga Perković, Karin A. Dahmen, Bruce W. Roberts, and James P. Sethna, *Comput. Sci. Eng. 1,* ***73*** (1993)

[13] James P. Sethna, Karin A. Dahmen, Christopher R. Myers *Crackling Noise, Nature Vol* ***410*** (2001)

[14] Perkovic O., Dahmen, K. A. Sethna, J. P., *Avalanches, Barkhausen noise, and plain old criticality. Phys. Rev. Lett.* ***75***, 4528–4531 (1995).

[15] Karin Dahmen and James P. Sethna, *Phys. Rev. B 53* ***22*** 872-905 (1996)

[16] Aaron Clauset, Cosma Rohilla Shalizi, M. E. J. Newman, *SIAM Review* ***51***, 661-703 (2009)

[17] Francisco J. Pérez-Reche, Eduard Vives, *Phys. Rev. B* ***70***, 214422 (2004)